# Highly Thermal Stable and Efficient Organic Photovoltaic Cells with Crosslinked Networks Appending Open-Cage Fullerenes as Additives

*Chih-Ping Chen,* Chien-Yu Huang, and Shih-Ching Chuang**

**Highly thermal stable organic bulk heterojunction (OBHJ) photovoltaic cells are demonstrated with crosslinkable open-cage fullerenes (COF) as additives in the active layer. Partial incorporation of COF, ≈10–15 wt% with weight ratio of P3HT:$PC_{61}BM$ = 1:0.9, builds up three-dimensional local borders upon heating treatment at 150 °C for 10 min. This process induces crosslinking chemical reaction through activating the styryl moiety in COF and reduces phase aggregation rates of fullerenes materials. Supported by statistics of devices degradation data analysis and optical microscopy study, the devices with COF show longer lifetime with keeping their efficiency ($t$ = 144 h) under accelerated heating test at 150 °C, while PCE of normal devices without COF drop dramatically. These results demonstrate that the thermally crosslinkable COF is an excellent additive for highly thermal stable and durable OPVs applications.**

## 1. Introduction

The emerged field of organic photovoltaics (OPVs) is receiving a great deal of attention because it covers features of inexpensiveness, large-area fabrication, short energy-payback times, and roll-to-roll processing.[1] Improved photo conversion efficiency (PCE) of organic bulk heterojunction (OBHJ) technology through the innovation of n- and p-type materials and device engineering has also been demonstrated.[2] Despite of its current high efficiency up to 10.6%, the stability of OPVs has been constantly concerns for stepping into future marketing.[3] OPV devices composing of an active layer through solution processed BHJ blends based on a bicontinuous interpenetrating donor (D) and acceptor (A) network require optimal phase segregation with the scale of exciton diffusion length of 10–20 nm.[4] The blending morphology critically determines cell performance and can be controlled by the post–treatments (kinetic factors); for instances, thermal annealing,[5] additives control[6] and solvent annealing.[7] Therefore, the optimal morphology is kinetically locked and merely metastable and that the blends readily move toward a more thermodynamically stable state spontaneously. For practical applications, the device must afford for treatment at elevated temperature under constant thermal cycles.[8] Under this circumstance, the conjugated polymers continue to form better packing or further crystallization, while the fullerenes tend to diffuse into large aggregates or clusters or even single crystals.[9] As a result, the blends will reach thermodynamic equilibriums to form microphase segregation and the devices performance deteriorate.[6a,10] Consequently, sufficient device thermal stability is considered to be a significant challenge for commercialization.

Previous efforts to improve the thermal stability of OPV devices include addition of morphology compatibilizer,[11] chemically cross-linked fullerenes[9b,12] or conjugated polymers.[13] The approach with in situ chemical crosslinking in BHJ blended films had shown significant impact on enhancement of morphological stability. For instances, Hsu and Cheng et al. have first demonstrated thermally stable devices with stability over 25 h heating at 150 °C based on styryl-modified [6,6]-phenyl-$C_{61}$-butyric acid methyl ester (**$PC_{61}BM$**) derivatives.[9b] Our interests in developing non-**PCBM**-based fullerene derivatives for OPVs applications led us to explore new functional materials using open-cage fullerenes to this field.[14] The utilized open-cage fullerenes feature ease of synthetic availability in good yields from initial cycloaddition of diazenes with $C_{60}$ and later direct functionality modification for appending crosslinkable styryl moieties. The advantages of incorporating open-cage fullerenes in OPVs are reflected from their structural stability owing to their lack of strained three-membered ring moiety while compared with **$PC_{61}BM$**. In this paper, we wish to report an open-cage fullerene derivative possessing styryl-functionality, denoted as **COF**, and evaluate its stability upon being partially embedded in the active layers with

Prof. C.-P. Chen
Department of Materials Engineering
Ming Chi University of Technology
84 Gunjuan Road, Taishan, New Taipei City
243, Taiwan, R.O.C.
E-mail: cpchen@mail.mcut.edu.tw
Prof. C.-P. Chen
Battery Research Center of Green Energy
Ming Chi University of Technology
84 Gunjuan Road, Taishan
New Taipei City, 243, Taiwan R.O.C.
C.-Y. Huang, Prof. S.-C. Chuang
Department of Applied Chemistry
National Chiao Tung University
Hsinchu, Taiwan, R.O.C. 30010
E-mail: jscchuang@faculty.nctu.edu.tw

**DOI: 10.1002/adfm.201401735**

poly(3-hexylthiophene), P3HT, in the devices. The crosslinking reaction can be induced by heating at 150 °C for ≈10 min that triggers polymerization of styryl groups[9b]—which leads to an interpenetrating networks appending open-cage fullerene molecules. The addition of **COF** may bring closer intermediacy effect between $\mathbf{PC_{61}BM}$ and P3HT through the two thienyl moieties and fullerene of **COF**. The concept of "Like dissolves like" interprets the purpose of using a fullerene derivative with thienyl functionality as shown in **COF** since the fullerene moiety in **COF** controls intimacy with $\mathbf{PC_{61}BM}$ and thienyl moiety plays intimacy with P3HT through van der Waals interaction. This doubled control will likely slow down the donor and acceptor phase segregation. Further advantage utilizing this styryl-bearing **COF** allows radical addition of styryl moiety to the $\mathbf{PC_{61}BM}$ or **COF** itself. This process will lead to partial covalently bonded fullerene networks that slow down aggregation and thereby stabilize the morphology accordingly.[15] The such formed BHJ cell slows down further diffusion and crystallization of fullerene molecules macroscopically.[9b] The devices with **COF** as an additive in the active layer have shown extremely high thermal stability under long-term accelerated thermal treatment at 150 °C for over 144 h with constantly high power conversion efficiency (PCE) of 3.2%—demonstrating **COF** as relatively superior crosslinking additives than that resulted from modified $\mathbf{PC_{61}BM}$.[9b]

## 2. Results and Discussion

The synthesis of the **COF** was described in **Scheme 1**. Initially, diazene **3** was prepared by an inverse electron demand Diels-Alder reaction of 3,6-di(thiophen-2-yl)-1,2,4,5-tetrazine (**1**) with methyl hex-5-enoate (**2**) in 74% yield. Cycloaddition of diazene **3** with $C_{60}$ followed by nitrogen extrusion in situ provided open-cage fullerene **4** in 45% yield (82% based on converted $C_{60}$). Transesterification of **4** with thermally linkable styryl moiety through carboxylic acid **5** gave **COF** (**7**). **COF** displayed interesting electrochemical properties. We used cyclic voltammetry (CV), differential pulse voltammetry (DPV), and Osteryoung square wave voltammetry (OSWV) to examine the redox properties of **COF**. Although open-cage fullerene **4** exhibited its first half-wave reduction potential ($^1E_{1/2}$) at –1.22 V, the $^1E_{1/2}$ of **COF** appeared at –1.24 V at a scan rate of 20 $mVs^{-1}$ by CV study (see the Supporting Information, SI). This has indicated that appendage of a crosslinkable styryl moiety to the open-cage fullerene **4** alters its lowest unoccupied molecular orbital (LUMO) to a slightly higher energy level than $\mathbf{PC_{61}BM}$, indicating that incorporation of **COF** in the active layer will not alter the open-circuit voltage ($V_{oc}$) of cells greatly.

The OPVs with layered configurations of glass/ITO/PEDOT:PSS/active layer/Ca/Al were fabricated using methods same as those reported previously.[16] We monitored the device performance with variable P3HT–$\mathbf{PC_{61}BM}$–**COF** ratios to determine the optimal compositions. The layers of Ca (30 nm) and Al (100 nm) were deposited thermally under vacuum. After encapsulating the devices with UV-curing glue, the *I–V* characteristics of devices were measured in air. The optimal **COF** composition ratios were found to be 10 to 15 wt%. The devices with **COF** embedded in the active layer, denoted as **COF** devices, were fabricated by spin-casting a blended *ortho*-dichlorobenzene solution containing P3HT, $\mathbf{PC_{61}BM}$ and **COF** with concentration of 18 $mgmL^{-1}$ for P3HT (weight ratio of P3HT:$\mathbf{PC_{61}BM}$:**COF** = 1:0.9:0.1) at a spin rate of 450 rpm for 30 s. We noted that the short circuit current density ($J_{sc}$) of the cell decreased upon increasing the **COF** ratio in the active layer. For comparison, the normal devices with P3HT:$\mathbf{PC_{61}BM}$ = 1:0.9 without **COF** were fabricated using the same condition. **Table 1** showed the OPV performance of normal and **COF** devices after thermal annealing at 150 °C for 10 min. The normal devices exhibited PCE of 3.78 ± 0.14% under AM 1.5G irradiation (100 $mWcm^{-2}$) with $J_{sc}$, $V_{oc}$, and fill factor (FF) of 9.40 ± 0.19 mA $cm^{-2}$, 0.61 ± 0.01 V and 0.66 ± 0.01, respectively, and those for the

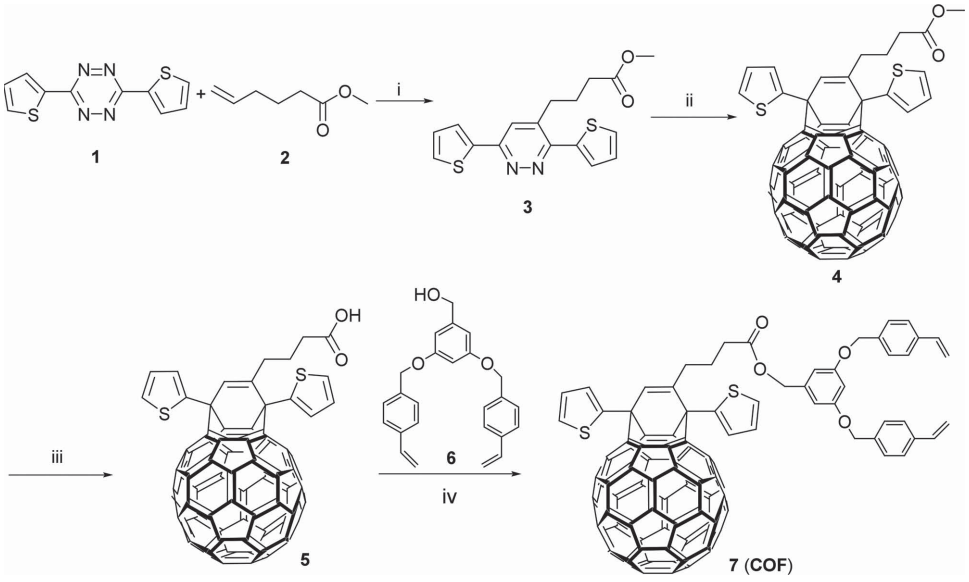


**Scheme 1.** Synthesis of crosslinkable open-cage fullerene monomer **7** (**COF**). i) *o*-xylene, 140 °C, 24 h, then $O_2$, 24 h, 140 °C, 74%; ii) 1-chloro-naphthalene, 270 °C, 26 h, $N_2$, 45% (82% based on converted $C_{60}$); iii) HCl, AcOH, chlorobenzene, reflux, 24 h, 76%; iv) EDC, DMAP, *o*-DCB, 0 °C to rt, 49%.

**Table 1.** Photovoltaic parameters of normal (A) and COF devices (B) as functions of heating time at 150 °C.

| Devices | Time | $J_{sc}$ [mA cm$^{-2}$] | $V_{oc}$ [V] | FF | $PCE_{ave}$ [%][c)] | $PCE_{best}$ [%][c)] |
|---|---|---|---|---|---|---|
| A | 10 min[a)] | 9.40 ± 0.19 | 0.61 ± 0.01 | 0.66 ± 0.01 | 3.78 ± 0.14 | 3.93 |
| A | 6 h[a)] | 9.44 ± 0.10 | 0.61 ± 0.001 | 0.65 ± 0.004 | 3.75 ± 0.06 | 3.85 |
| A | 18 h[a)] | 8.58 ± 0.18 | 0.62 ± 0.002 | 0.64 ± 0.004 | 3.42 ± 0.09 | 3.55 |
| A | 24 h[a)] | 7.66 ± 0.69 | 0.61 ± 0.01 | 0.63 ± 0.02 | 2.92 ± 0.36 | 3.50 |
| A | 96 h[a)] | 2.16 ± 0.11 | 0.60 ± 0.004 | 0.46 ± 0.005 | 0.60 ± 0.03 | 0.65 |
| A | 144 h[a)] | 0.96 ± 0.10 | 0.58 ± 0.01 | 0.42 ± 0.004 | 0.23 ± 0.03 | 0.29 |
| B | 10 min[b)] | 7.93 ± 0.30 | 0.60 ± 0.001 | 0.64 ± 0.01 | 3.08 ± 0.14 | 3.22 |
| B | 6 h[b)] | 8.68 ± 0.06 | 0.61 ± 0.002 | 0.66 ± 0.01 | 3.51 ± 0.07 | 3.60 |
| B | 18 h[b)] | 8.60 ± 0.31 | 0.61 ± 0.001 | 0.67 ± 0.01 | 3.51 ± 0.13 | 3.63 |
| B | 24 h[b)] | 8.94 ± 0.08 | 0.61 ± 0.001 | 0.65 ± 0.02 | 3.53 ± 0.12 | 3.70 |
| B | 96 h[b)] | 8.64 ± 0.21 | 0.61 ± 0.01 | 0.64 ± 0.01 | 3.36 ± 0.05 | 3.44 |
| B | 144 h[b)] | 7.67 ± 0.17 | 0.60 ± 0.001 | 0.66 ± 0.004 | 3.06 ± 0.07 | 3.16 |

[a)]Normal devices; [b)]**COF**-derived devices. [c)]The PCEs were resulted from eight independent devices.

**COF** derived devices showed PCE of 3.08 ± 0.14% with $J_{sc}$, $V_{oc}$, and FF of 7.93 ± 0.3 mAcm$^{-2}$, 0.60 ± 0.00 V, and 0.64 ± 0.01, respectively. It was evident that the additive **COF** showed a slightly decrease of device performance due to the lower value of $J_{sc}$ and little effect on $V_{oc}$.

Our primary interests in revealing the relative stability of **COF** devices versus normal devices statistically led us to study the devices degradations with time. The degradation of normal and **COF** devices under accelerated thermal annealing conditions was initially investigated at 65 °C based upon International Summit on OPV Stability (ISOS-3) standards. However, we were not able to draw assertive conclusion of their relative stability since the **COF** devices barely showed degradation under long-term operation (1000 h, Figure S1, SI). Therefore, we carried out degradation experiments at 150 °C from which we observed meaningful degradations on **COF** devices.[17] Hsu and Cheng et al. ever demonstrated the crosslinking technique to trigger polymerization of styryl groups at 150 °C,[9b] leading to interpenetrating networks to restrain diffusion and crystallization of $PC_{61}BM$ molecules in the active layer macroscopically. We investigated the minimal temperature to trigger crosslinking of the styryl moiety on **COF** by differential scanning calorimetry (DSC). In the first scanning cycle, a broad exothermic peak approximately embarking at 140 °C was observed (Figure S2a, SI). After the first heating cycle, we observed no thermal transition on the second DSC scan and concluded that complete crosslinking of the **COF** was furnished in the first run.[18] Further, the vibrational stretching of the styryl group (C = C) at 1611 cm$^{-1}$ vanished after annealing at 150 °C for 30 min (Figure S2b, SI), reflecting the occurrence of the crosslinking reaction.[18,19] In order to systematically and correctly evaluate the capability of **COF** for stabilizing the devices, we eliminated the effects from the instability of top electrodes contacts. Thus, the OPV devices were thermally annealed at 150 °C inside a glove box for reduction of the decay factors by oxygen and water with various periods of time prior to deposition of the top electrodes on devices. **Figure 1** and Table 1 showed the summarized PCEs as a function of time for studied devices. The PCEs of these fabricated devices were reproducible and exhibited variations of <5% of eight individual OPV devices. The normal devices remained 90% of their initial PCEs after 24 h annealing time at 150 °C, indicating the thermal stability of P3HT and $PC_{61}BM$ BHJ devices in certain extents (Figure 1a). However, the normal cells showed ca. 90% decrease of PCEs under extended thermal treatments ($t$ = 96 h). In contrast, the **COF** cell showed ≈10% PCE enhancement after thermal treatments (Figure 1b,c). The highest PCE of 3.7% was achieved after annealing for 24 h and the device remained ≈95% of its initial efficiency value under accelerated thermal conditions for 144 h.

We studied the morphologies of the blend films evolved over accelerated process with optical microscopy (OM) to characterize the phenomena.[9b,13c,20] For direct comparison, we prepared films for OM analysis under the same conditions used for device fabrication. **Figure 2** displayed the OM images of blend film with and without **COF** after various thermal annealing periods. As shown in Figure 2a, the morphology of normal blended devices developed dramatically upon annealing. The thin film with less than 10 min annealing time was featureless and did not exhibit any large area aggregations. Nevertheless, the low-molecular-weight components, fullerenes, preferred to diffuse into large aggregates under elevated temperatures. When the heating time was extended to over 6 h, the normal blend films showed large 20-μm sizable aggregates. The formed dendritic-like aggregates during the annealing process were attributed to the crystallization of $PC_{61}BM$.[9b,10,13c] The device performance was relevant to this anomalous aggregation behavior. The observed PCEs of the normal cell slightly decreased from 3.78 ± 0.14% ($t$ = 10 min) to 3.75 ± 0.06% ($t$ = 6 h) upon small amounts of aggregates appeared. Further decrease of 10% of PCE was observed ($t$ = 24 h) while the size of aggregates increased from 20 to 30 μm. The size and the amount of aggregates steeply increased when the treatment time was further extended. In contrast, the **COF**-containing film barely showed an increase in fullerene aggregation while comparing the morphology at the initial heating time of 10 min

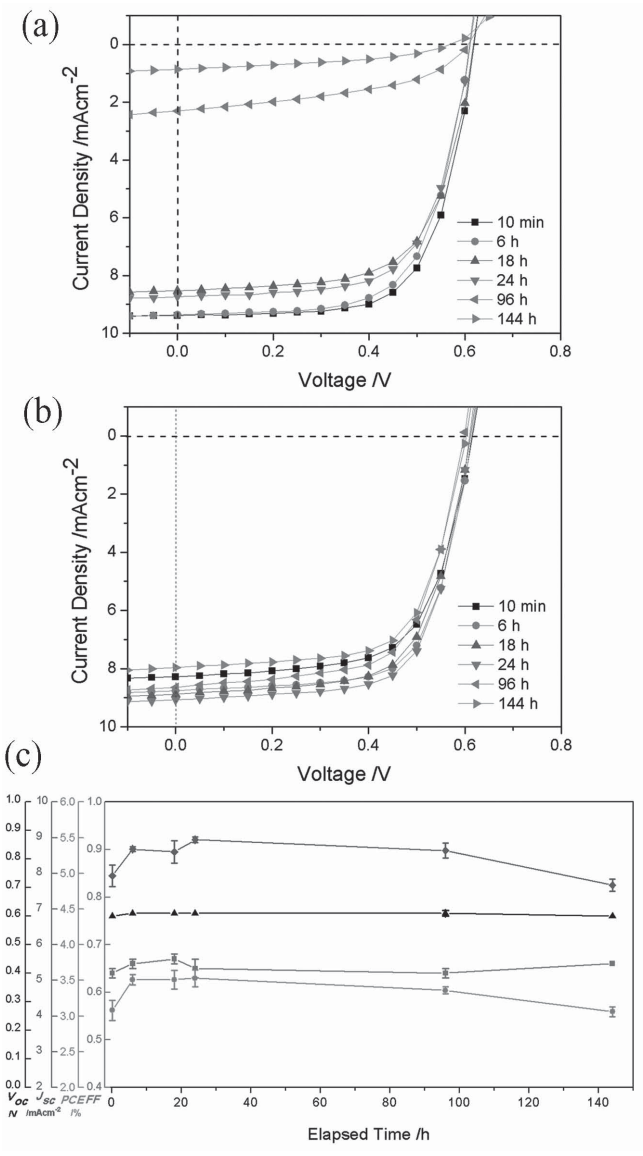


**Figure 1.** *J–V* characteristics of OPV devices based on the blend films of P3HT:**$PC_{61}BM$**, a) w/o and b) w/ **COF** under accelerated condition at 150 °C for various times. c) Photovoltaic performance of **COF**-derived cells tested at 150 °C with various annealing time in the dark under $N_2$. (▲): $V_{oc}$; (◆):$J_{sc}$; (●): PCE; (■): FF.

and that at 24 h (Figure 2b). The smaller sizable aggregates were observed at longer heating time; as a result, the PCE of corresponding device increased slightly. One may doubt that the crosslinkable additive, **COF**, may not undergo crosslinking reaction due to its lower content of 10 to 15% in the active layer; however, we did not observe any spot corresponding to **COF** by thin-layered chromatography analysis after dissolving the films of active layers in dichloromethane after 6 h annealing process. We only observed a spot corresponding to **$PC_{61}BM$** and a baseline spot that may correspond to polymerized materials incorporating **COF**. In addition, Pozzo et al. have demonstrated that controlled addition of $C_{60}$ in the P3HT/**$PC_{61}BM$** layer induced faster nucleation of **$PC_{61}BM$** to form smaller **$PC_{61}BM$** crystallites with simultaneous increase of the devices stability.[21] Suppose our **COF** behaved as $C_{60}$ that could have induced faster nucleation process of **$PC_{61}BM$** as that in Pozzo's study, we should have observed dramatic changes on the morphology under different ratio loadings of **COF** in annealing experiments. However, the morphology of the **COF**-derived blend remained at similar extent upon thermally annealed at 150 °C for $t$ = 1/6, 6, 18 and 24 h in our OM images of **COF**-derived films with 10 and 20 wt% loading (Figure 2 and SI Figure S3). This may be due to the delay of **$PC_{61}BM$** nucleation or more likely the excellent ability of **COF** to chemically fix the morphology by crosslinking, leading to increase higher density of crystallites appearing at longer annealing period ($t$ = 96 h). The occurrence of local crosslinking networks could suppress the rates of crystallization of **$PC_{61}BM$** instead of reducing the average crystallite size of the fullerene through nucleation effect.

The performance of the two studied devices along thermal annealing time can be accounted with UV–Vis absorption and photoluminescence spectra respectively. It has been shown that thermal annealing process can increase the mesoscopic order and crystallinity of P3HT and **$PC_{61}BM$** blend film, and the charge transportation of holes and electrons will be enhanced accordingly.[22] Nano-scale morphology phase segregation with semicrystalline order of both components was desirable architecture for the blends to achieve highly efficient photovoltaics.[23] The extended thermal annealing time allowed both components to increase their crystallinity. This behavior can be monitored by UV–vis absorption at specific wavelengths and provided supporting evidence to interpret the phenomena.[6b] Figure S4 (SI) showed the absorption spectra of normal and **COF**-blend films at different annealing times. Three typical absorption peaks, located at 515, 550, and 610 nm, were attributed to the P3HT absorption peaks and were known to be relevant to the vibronic splitting of the $\pi$–$\pi^*$ transition, and their extents of crystallinity.[5,16a] Further, the absorption peak at 610 nm was associated to the inter-chain $\pi$–$\pi^*$ transition of P3HT and it reflected significant degree of structural ordering. The growth of three vibronic shoulders at 515, 550, and 610 nm was found for both devices under extended annealing times. Due to strong interchain–interlayer interactions or better packing of polymer P3HT, the morphology of P3HT gradually shifted from semi-crystalline to more crystalline state—a significant behavior for the normal device. Nevertheless, the **$PC_{61}BM$** diffusion and aggregation played the other determinant rule for the performance of normal devices since the crystallization process of P3HT accompanied with significant blend microphase segregation. Consequently, it was evident that the morphology of devices without **COF** deteriorated gradually (Figure 2a, $t$ = 10 min to 144 h) and the OPV performance decreased (Table 1 and Figure 1). In contrast, the diffusion and crystallization of **$PC_{61}BM$** were almost suppressed for the **COF**-device. The crosslinked **COF** built local borders that slowed down the extensive diffusion of **$PC_{61}BM$** and large-scale crystallization. Consequently, the P3HT can go further for self-assembling and the enhanced performance (3.7%, Table 1) of **COF**-device was obtained after annealing at 150 °C for 24 h.

Due to ultrafast photoinduced charge transfer within donor–acceptor (D–A) interfaces,[24] the photoluminescence (PL) of the

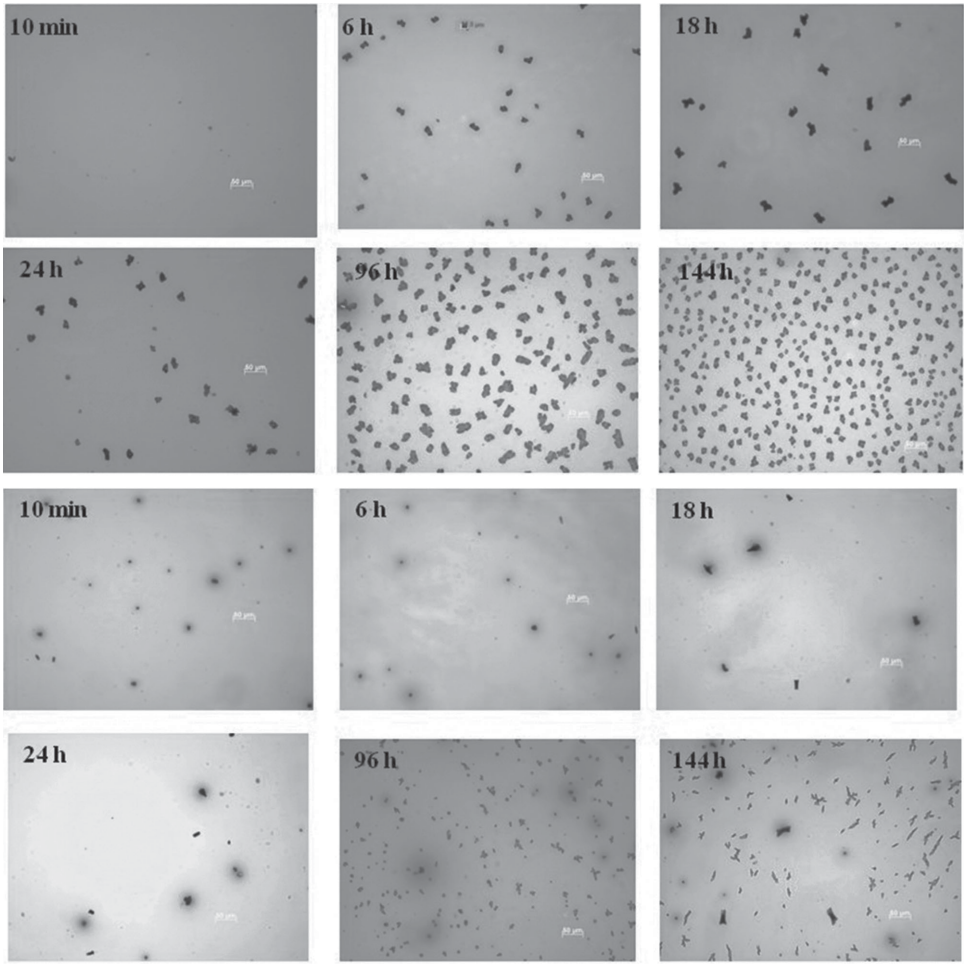


**Figure 2.** Optical microscopy images of a) the normal and b) **COF**-derived blend films under accelerated condition at 150 °C for various lengths of times. (Scale bar: 50 micrometers.)

blend films could almost be quenched for a well-defined OPV blend morphology and thus it provided solid evidence for confirmation of the morphology induced instability in the devices. It was known that a large-scale phase separation greater than the diffusion length of excitons, typically 20 nm, photoluminescence will take place.[6a,24] Figure S5 showed PL spectra of the blend films with and without **COF** at 150 °C as a function of time respectively. The blend films with **COF** remained to exhibit PL quenching at $t$ = 144 h as the same magnitude of PL at $t$ = 6 h. In contrast, the PL of devices without **COF** increased with time since the active layer morphology degraded from optimal state upon long-term annealing, corroborating the fact of macro-phase segregation of P3HT from **$PC_{61}BM$**. This notion was attributed to decay of excitons through radiative relaxation when domain size of P3HT-rich or fullerene-rich phases was greater than the diffusion length of excitons in the active layer; thereof, the large population of generated excitons cannot reach the D–A interfaces. Due to large phase segregation, PL was observed nearly as twice as large for normal devices after extended annealing process—consistent with the degraded performance of OPVs.

Based on results of accelerated testing, the lifetime of OPVs devices has been predicted to be stable for years under stress testings such as elevated temperatures, cyclic or periodic mechanical and/or electrical stresses and concentrated light.[25] Typically, the increase of temperature was an accelerating factor for the aging mechanism.[25b] Brabec et al. have suggested a delicate approach to evaluate the lifetime of photovoltaic devices at variable temperature.[26] However, Krebs et al. have pointed out that[25b,27] the used Arrhenius model was rather complex and it has not been well studied by the OPV community. Our preliminary results have indicated that addition of this new crosslinkable material, **COF**, allowed the device to exhibit good stability under inert conditions (150 °C; concentration of $O_2$ and $H_2O$ < 10 ppm) with omission of the top electrode contact issue (Ca/Al).

To study the performance of **COF** with a typical low bandgap conjugated polymer, Poly[[4,8-bis[(2-ethylhexyl)oxy] benzo[1,2-b:4,5-b′]dithiophene-2,6-diyl][3-fluoro-2-[(2-ethyl hexyl)carbonyl]thieno[3,4-b]thiophenediyl]] (PTB7), we fabricated the PTB7/**$PC_{71}BM$**, PTB7/**$PC_{61}BM$** and PTB7/**$PC_{61}BM$/COF** devices under the same fabrication condition. The detailed process for PTB7/**$PC_{61}BM$/COF** device was by spin-casting a

blended chlorobenzene solution containing PTB7, **$PC_{61}BM$** and **COF** with concentration of 10 mgmL$^{-1}$ for PTB7 (weight ratio of PTB7:**$PC_{61}BM$**:**COF** = 1:1.5:0.1) and 3 vol% of 1,8-diiodooctane (DIO) as additives at a spin rate of 1200 rpm for 30 s. As PTB7 is a less crystalline polymer than P3HT, the morphology study showed that the PTB7/**PCBM** blend featured relatively smaller phase segregations where **PCBM** domains were better interpenetrated within the polymers than that in P3HT/**PCBM** blend.[28] Wantz et al. have observed a significant drop of device performance due to occurrence of micro-phase fullerene crystals after thermal annealing at 150 °C for 16 h for PTB7-based blends devices since PTB7/**PCBM** blends were thermally unstable than P3HT/**PCBM**.[28a] As shown in Table S1 (SI), we observed similar phenomenon—the PCEs drop from 6.1 to 1.5% and 4.9 to 0.1% for the PTB7/**$PC_{71}BM$** and PTB7/**$PC_{61}BM$**-based devices after they were annealed at 150 °C for 18 h, respectively. While addition of 10 wt% of **COF** to PTB7/**$PC_{61}BM$** device, the device performance degraded from 5.0 to 3.2% (Table S1) under the same stress conditions, in which FF primarily contributed to the loss of PCEs. Future optimization will be focusing on other high-performance donor polymers, optimal concentrations and modification of **COF** structure to demonstrate highly stable and high PCE OPV devices.

## 3. Conclusions

In summary, we have demonstrated highly thermal stable organic solar cells with crosslinkable open-cage fullerenes as additives for building up partial local borders that reduced phase aggregation rates of fullerenes materials. Supported by statistical data analysis and optical microscopy observation, we have confirmed that the phase aggregation of OPVs with **COF** as additives in the active was slowed down. The resulting devices showed longer lifetime than a normal device without crosslinkable open-cage fullerenes as additives under accelerated heating test at 150 °C. These results have demonstrated that the thermally crosslinkable **COF** was an excellent additive for highly thermal stable and durable OPVs applications.

## 4. Experimental Section

*Measurement and Characterization*: All chemicals were purchased from Aldrich and used as received unless otherwise specified. $^1$H NMR spectra were recorded using a Bruker spectrometer. Absorption spectra were recorded on a Perkin–Elmer Lambda 950 UV–Vis spectrophotometer. Differential scanning calorimetry (DSC) was measured with a TA instrument (TA Q20) at a heating rate of 10 °C min$^{-1}$. Fourier transform infrared (FT-IR) spectra were recorded with a Perkin Elmer infrared spectrometer. Current–voltage (*I*–*V*) curves of the OPVs devices were measured using a computer-controlled Keithley 2400 source measurement unit (SMU) equipped with a Peccell solar simulator under the illumination of AM 1.5 (100 mW cm$^{-2}$). The illumination intensity was calibrated using a standard Si photodiode detector equipped with a KG-5 filter. The output photocurrent was adjusted to match the photocurrent of the Si reference cell to obtain a power density of 100 mWcm$^{-2}$. After encapsulation, all devices were operated under an ambient atmosphere at 25 °C.

*Photovoltaic Cell Fabrication and Testing*: All the bulk-heterojunction OPV cells were prepared using the following device fabrication procedure:[6a,14] The glass/indium tin oxide (ITO) substrates [Sanyo, Japan (8Ω/□)] were sequentially patterned lithographically, cleaned with detergent, ultrasonicated in acetone and isopropyl alcohol, dried on a hot plate at 120 °C for 5 min, and treated with oxygen plasma for 5 min. Poly(3,4-ethylene-dioxythiophene):poly(styrene-sulfonate) (PEDOT:PSS, Baytron P-VP AI4083) was passed through a 0.45-μm filter before being deposited on ITO at a thickness of ≈30 nm by spin-coating at 3000 rpm in air and then dried at 150 °C for 30 min inside a glove box. A blend of 1-(3-methoxycarbonyl)propyl-1-phenyl-[6,6]-$C_{61}$ (**$PC_{61}BM$**) and the P3HT [0.9:1 (w/w), 18 mg mL$^{-1}$ in *o*-DCB] was stirred overnight in *o*-DCB, filtered through a 0.2-μm poly(tetrafluoroethylene) (PTFE) filter, and then spin-coated (500–1000 rpm, 30 s) on top of the PEDOT:PSS layer. The device was completed by depositing a 30-nm-thick layer of Ca and a 100-nm-thick layer of Al at pressures less than $10^{-6}$ Torr. The active area of the device was 4 mm$^2$. Finally the cell was encapsulated using UV-curing glue (Nagase, Japan)

## Supporting Information

Supporting Information is available from the Wiley Online Library or from the author.

## Acknowledgements

The authors thank the Ministry of Economic Affairs and Ministry of Science and Technology (MOST 101–2113-M-131–001-MY2; MOST 96–2113-M-009–028-MY2; MOST 103–2113-M-009–017), Taiwan, for supporting this research financially and Industrial Technology Research Institute (ITRI) for providing the facility.

Received: May 29, 2014
Revised: September 3, 2014
Published online: October 27, 2014

[1] a) M. Jørgensen, K. Norrman, S. A. Gevorgyan, T. Tromholt, B. Andreasen, F. C. Krebs, *Adv. Mater.* **2012**, *24*, 580–612; b) N. Espinosa, M. Hosel, D. Angmo, F. C. Krebs, *Energy Environ. Sci.* **2012**, *5*, 5117–5132; c) C.-P. Chen, Y.-D. Chen, S.-C. Chuang, *Adv. Mater.* **2011**, *23*, 3859–3863; d) W. Li, K. H. Hendriks, W. S. Roelofs, Y. Kim, M. M. Wienk, R. A. Janssen, *Adv. Mater.* **2013**, *25*, 3182–3186; e) H. J. Son, L. Lu, W. Chen, T. Xu, T. Zheng, B. Carsten, J. Strzalka, S. B. Darling, L. X. Chen, L. Yu, *Adv. Mater.* **2013**, *25*, 838–843; f) Q. Shi, P. Cheng, Y. Li, X. Zhan, *Adv. Energy Mater.* **2012**, *2*, 63–67.

[2] a) Y.-C. Chen, C.-Y. Yu, Y.-L. Fan, L.-I. Hung, C.-P. Chen, C. Ting, *Chem. Commun.* **2010**, *46*, 6503–6505; b) X. Li, W. C. H. Choy, L. Huo, F. Xie, W. E. I. Sha, B. Ding, X. Guo, Y. Li, J. Hou, J. You, Y. Yang, *Adv. Mater.* **2012**, *24*, 3046–3052; c) X. Guo, M. Zhang, J. Tan, S. Zhang, L. Huo, W. Hu, Y. Li, J. Hou, *Adv. Mater.* **2012**, *24*, 6536–6541; d) J. You, L. Dou, Z. Hong, G. Li, Y. Yang, *Prog. Polym. Sci.* **2013**, *38*, 1909–1928; e) M. C. Scharber, N. S. Sariciftci, *Prog. Polym. Sci.* **2013**, *38*, 1929–1940; f) Q. Xu, F. Wang, D. Qian, Z. a. Tan, L. Li, S. Li, X. Tu, G. Sun, X. Hou, J. Hou, Y. Li, *ACS Appl. Mater. Interfaces* **2013**, *5*, 6591–6597; g) Z. a. Tan, W. Zhang, Z. Zhang, D. Qian, Y. Huang, J. Hou, Y. Li, *Adv. Mater.* **2012**, *24*, 1476–1481; h) Z. a. Tan, S. Li, F. Wang, D. Qian, J. Lin, J. Hou, Y. Li, *Sci. Rep.* **2014**, *4*, 4691.

[3] a) Z. He, C. Zhong, S. Su, M. Xu, H. Wu, Y. Cao, *Nat. Photonics* **2012**, *6*, 591–595; b) J. You, L. Dou, K. Yoshimura, T. Kato, K. Ohya, T. Moriarty, K. Emery, C.-C. Chen, J. Gao, G. Li, Y. Yang, *Nat.*

*Commun.* **2013**, *4*, 1446; c) Q. Gan, F. J. Bartoli, Z. H. Kafafi, *Adv. Mater.* **2013**, *25*, 2385–2396; d) F. C. Krebs, N. Espinosa, M. Hösel, R. R. Søndergaard, M. Jørgensen, *Adv. Mater.* **2014**, *26*, 29–39.

[4] Y.-J. Cheng, S.-H. Yang, C.-S. Hsu, *Chem. Rev.* **2009**, *109*, 5868–5923.

[5] C.-P. Chen, C. Luo, C. Ting, S.-C. Chuang, *Chem. Commun.* **2011**, *47*, 1845–1847.

[6] a) S.-H. Chan, Y.-S. Hsiao, L.-I. Hung, G.-W. Hwang, H.-L. Chen, C. Ting, C.-P. Chen, *Macromolecules* **2010**, *43*, 3399–3405; b) S.-H. Chan, C.-S. Lai, H.-L. Chen, C. Ting, C.-P. Chen, *Macromolecules* **2011**, *44*, 8886–8891.

[7] C.-P. Chen, Y.-C. Chen, C.-Y. Yu, *Polym. Chem.* **2013**, *4*, 1161–1166.

[8] a) N. Espinosa, R. Garcia-Valverde, F. C. Krebs, *Energy Environ. Sci.* **2011**, *4*, 1547–1557; b) N. Espinosa, R. García-Valverde, A. Urbina, F. C. Krebs, *Sol. Energy Mater. Sol. Cells* **2011**, *95*, 1293–1302.

[9] a) X. Yang, J. K. J. van Duren, R. A. J. Janssen, M. A. J. Michels, J. Loos, *Macromolecules* **2004**, *37*, 2151–2158; b) Y.-J. Cheng, C.-H. Hsieh, P.-J. Li, C.-S. Hsu, *Adv. Funct. Mater.* **2011**, *21*, 1723–1732.

[10] S. Nilsson, A. Bernasik, A. Budkowski, E. Moons, *Macromolecules* **2007**, *40*, 8291–8301.

[11] K. Sivula, C. K. Luscombe, B. C. Thompson, J. M. J. Frechet, *J. Am. Chem. Soc.* **2006**, *128*, 13988–13989.

[12] a) J.-F. Nierengarten, S. Setayesh, *N. J. Chem.* **2006**, *30*, 313–316; b) M. Drees, H. Hoppe, C. Winder, H. Neugebauer, N. S. Sariciftci, W. Schwinger, F. Schaffler, C. Topf, M. C. Scharber, Z. Zhu, R. Gaudiana, *J. Mater. Chem.* **2005**, *15*, 5158–5163.

[13] a) C.-Y. Nam, Y. Qin, Y. S. Park, H. Hlaing, X. Lu, B. M. Ocko, C. T. Black, R. B. Grubbs, *Macromolecules* **2012**, *45*, 2338–2347; b) B. Gholamkhass, S. Holdcroft, *Chem. Mater.* **2010**, *22*, 5371–5376; c) B. J. Kim, Y. Miyamoto, B. Ma, J. M. J. Fréchet, *Adv. Funct. Mater.* **2009**, *19*, 2273–2281; d) S. Miyanishi, K. Tajima, K. Hashimoto, *Macromolecules* **2009**, *42*, 1610–1618; e) D. Qian, Q. Xu, X. Hou, F. Wang, J. Hou, Z. a. Tan, *J. Polym. Sci. Part A: Polym. Chem.* **2013**, *51*, 3123–3131.

[14] C.-P. Chen, Y.-W. Lin, J.-C. Horng, S.-C. Chuang, *Adv. Energy Mater.* **2011**, *1*, 776–780.

[15] T. Cao, S. E. Webber, *Macromolecules* **1995**, *28*, 3741–3743.

[16] a) C.-Y. Liao, C.-P. Chen, C.-C. Chang, G.-W. Hwang, H.-H. Chou, C.-H. Cheng, *Sol. Energy Mater. Sol. Cells* **2013**, *109*, 111–119; b) C.-P. Chen, H.-L. Hsu, *Macromol. Rapid Commun.* **2013**, *34*, 1623–1628.

[17] G. Griffini, J. D. Douglas, C. Piliego, T. W. Holcombe, S. Turri, J. M. J. Fréchet, J. L. Mynar, *Adv. Mater.* **2011**, *23*, 1660–1664.

[18] C.-H. Hsieh, Y.-J. Cheng, P.-J. Li, C.-H. Chen, M. Dubosc, R.-M. Liang, C.-S. Hsu, *J. Am. Chem. Soc.* **2010**, *132*, 4887–4893.

[19] a) Y.-J. Cheng, M. S. Liu, Y. Zhang, Y. Niu, F. Huang, J.-W. Ka, H.-L. Yip, Y. Tian, A. K. Y. Jen, *Chem. Mater.* **2007**, *20*, 413–422; b) F. Huang, Y.-J. Cheng, Y. Zhang, M. S. Liu, A. K. Y. Jen, *J. Mater. Chem.* **2008**, *18*, 4495–4509.

[20] M.-H. Liao, C.-E. Tsai, Y.-Y. Lai, F.-Y. Cao, J.-S. Wu, C.-L. Wang, C.-S. Hsu, I. Liau, Y.-J. Cheng, *Adv. Funct. Mater.* **2014**, *24*, 1418–1429.

[21] J. J. Richards, A. H. Rice, R. D. Nelson, F. S. Kim, S. A. Jenekhe, C. K. Luscombe, D. C. Pozzo, *Adv. Funct. Mater.* **2013**, *23*, 514–522.

[22] a) X. Yang, J. Loos, S. C. Veenstra, W. J. H. Verhees, M. M. Wienk, J. M. Kroon, M. A. J. Michels, R. A. J. Janssen, *Nano Lett.* **2005**, *5*, 579–583; b) F. Liu, Y. Gu, C. Wang, W. Zhao, D. Chen, A. L. Briseno, T. P. Russell, *Adv. Mater.* **2012**, *24*, 3947–3951.

[23] E. Verploegen, R. Mondal, C. J. Bettinger, S. Sok, M. F. Toney, Z. Bao, *Adv. Funct. Mater.* **2010**, *20*, 3519–3529.

[24] C.-P. Chen, S.-H. Chan, T.-C. Chao, C. Ting, B.-T. Ko, *J. Am. Chem. Soc.* **2008**, *130*, 12828–12833.

[25] a) C. H. Peters, I. T. Sachs-Quintana, J. P. Kastrop, S. Beaupré, M. Leclerc, M. D. McGehee, *Adv. Energy Mater.* **2011**, *1*, 491–494; b) M. O. Reese, S. A. Gevorgyan, M. Jørgensen, E. Bundgaard, S. R. Kurtz, D. S. Ginley, D. C. Olson, M. T. Lloyd, P. Morvillo, E. A. Katz, A. Elschner, O. Haillant, T. R. Currier, V. Shrotriya, M. Hermenau, M. Riede, K. R. Kirov, G. Trimmel, T. Rath, O. Inganäs, F. Zhang, M. Andersson, K. Tvingstedt, M. Lira-Cantu, D. Laird, C. McGuiness, S. Gowrisanker, M. Pannone, M. Xiao, J. Hauch, R. Steim, D. M. DeLongchamp, R. Rösch, H. Hoppe, N. Espinosa, A. Urbina, G. Yaman-Uzunoglu, J.-B. Bonekamp, A. J. J. M. van Breemen, C. Girotto, E. Voroshazi, F. C. Krebs, *Sol. Energy Mater. Sol. Cells* **2011**, *95*, 1253–1267.

[26] S. Schuller, P. Schilinsky, J. Hauch, C. J. Brabec, *Appl. Phys. A* **2004**, *79*, 37–40.

[27] S. A. Gevorgyan, M. Jørgensen, F. C. Krebs, *Sol. Energy Mater. Sol. Cells* **2008**, *92*, 736–745.

[28] a) L. Derue, O. Dautel, A. Tournebize, M. Drees, H. Pan, S. Berthumeyrie, B. Pavageau, E. Cloutet, S. Chambon, L. Hirsch, A. Rivaton, P. Hudhomme, A. Facchetti, G. Wantz, *Adv. Mater.* **2014**, *26*, 5831; b) Y. Liang, Z. Xu, J. Xia, S.-T. Tsai, Y. Wu, G. Li, C. Ray, L. Yu, *Adv. Mater.* **2010**, *22*, E135–E138.